# Residual stress determination in oxide layers at different length scales combining Raman spectroscopy and X-ray diffraction: Application to chromia-forming metallic alloys

Mathieu Guerain, Jean-Luc Grosseau-Poussard, Guillaume Geandier, Benoit Panicaud, Nobumichi Tamura, Martin Kunz, Catherine Dejoie, Jean-Sebastien Micha, Dominique Thiaudière, and Philippe Goudeau

Citation: Journal of Applied Physics **122**, 195105 (2017);

View online: https://doi.org/10.1063/1.4990146

View Table of Contents: http://aip.scitation.org/toc/jap/122/19

Published by the American Institute of Physics

JOURNAL OF APPLIED PHYSICS **122**, 195105 (2017)

# Residual stress determination in oxide layers at different length scales combining Raman spectroscopy and X-ray diffraction: Application to chromia-forming metallic alloys

Mathieu Guerain,[1,a)] Jean-Luc Grosseau-Poussard,[1,b)] Guillaume Geandier,[2,c)] Benoit Panicaud,[3,d)] Nobumichi Tamura,[4,e)] Martin Kunz,[4,f)] Catherine Dejoie,[5,g)] Jean-Sebastien Micha,[6,h)] Dominique Thiaudière,[7,i)] and Philippe Goudeau[8,j)]
[1]*LaSIE, UMR-CNRS - Université de La Rochelle, La Rochelle, France*
[2]*Institut Jean Lamour, CNRS-Université de Lorraine, Nancy, France*
[3]*LASMIS, CNRS-Université Technologique de Troyes, Troyes, France*
[4]*ALS-LBNL, Berkeley, California 94702, USA*
[5]*ESRF, Grenoble, France*
[6]*Univ. Grenoble Alpes, CNRS UMR SPrAM, BM32 at ESRF, Grenoble, France*
[7]*Synchrotron SOLEIL, Gif sur Yvette, France*
[8]*Pprime, CNRS-Université de Poitiers-ENSMA, Poitiers, France*

(Received 14 June 2017; accepted 31 October 2017; published online 21 November 2017)

In oxidizing environments, the protection of metals and alloys against further oxidation at high temperature is provided by the oxide film itself. This protection is efficient only if the formed film adheres well to the metal (substrate), i.e., without microcracks and spalls induced by thermomechanical stresses. In this study, the residual stresses at both macroscopic and microscopic scales in the oxide film adhering to the substrate and over the damaged areas have been rigorously determined on the same samples for both techniques. Ni-30Cr and Fe-47Cr alloys have been oxidized together at 900 and 1000 °C, respectively, to create films with a thickness of a few microns. A multi-scale approach was adopted: macroscopic stress was determined by conventional X-ray diffraction and Raman spectroscopy, while microscopic residual stress mappings were performed over different types of bucklings using Raman micro-spectroscopy and synchrotron micro-diffraction. A very good agreement is found at macro- and microscales between the residual stress values obtained with both techniques, giving confidence on the reliability of the measurements. In addition, relevant structural information at the interface between the metallic substrate and the oxide layer was collected by micro-diffraction, a non-destructive technique that allows mapping through the oxide layer, and both the grain size and the crystallographic orientation of the supporting polycrystalline metal located either under a buckling or not were measured. *Published by AIP Publishing.* https://doi.org/10.1063/1.4990146

## I. INTRODUCTION

In applications where processes are running at high temperatures and extreme environments, raising the operating temperature is a crucial key parameter to achieve higher efficiency, and thus economical benefit, as well as reduction of pollutants and $CO_2$ emission. Durability of oxidized metallic materials is therefore a major concern. For technological applications at high temperature, alloys mainly based on chromium and aluminum were developed to create, in oxidizing atmospheres, chromium oxide or alumina films providing a protection against further oxidation. One of the major problems that limit the use of these alloys is the loss of the protective character of the oxide films. Indeed, under many experimental conditions, the oxide film is no longer bonding to the substrate and various geometrical configurations of the debonded regions detrimental to the metal protection and due to residual stress relaxation can be observed (blisters, worm-like structures, buckles, spalls…).[1–4]

These behaviors give rise to numerous interesting physical and mechanical observations which need to be understood to optimize the efficiency of the oxide films. Attempts have been made to explain the delamination process by taking into account the compressive stress of the growing oxide film. It seems that the delamination patterns start from an initial debonded localized zone and involve crack propagation at the oxide/alloy interface, which leads to an increase in the size of the non-adherent zone. When a critical size is reached, with the help of the local stress, spalling can occur. However, the exact mechanisms inducing the increase of the buckle size and the occurrence of spalls are not completely understood. Indeed, the local stress value, mainly near the edge of a starting buckle, has to be known for calculating, for instance, the interface toughness distribution from modelling describing buckle formation and propagation.[5] The curvature of the debonded oxide film locally induces more compressive and more tensile stresses (either) in the upper

[a)]mathieuguerain@hotmail.com
[b)]jlgrouss@univ-lr.fr
[c)]guillaume.geandier@univ-lorraine.fr
[d)]benoit.panicaud@utt.fr
[e)]ntamura@lbl.gov
[f)]mkunz@lbl.gov
[g)]dejoie@esrf.fr
[h)]micha@esrf.fr
[i)]dominique.thiaudiere@soleil.fr
[j)]philippe.goudeau@cnrs.pprime.fr

and (or) lower film surfaces. This geometrical configuration locally modifies the stress level. Therefore, stress measurements need to be spatially resolved at the micron level (the length scale of the debonded features).

Chromium based alloys oxidized at high temperature develop a continuous $\alpha$-$Cr_2O_3$ chromium oxide (chromia) scale at the top surface which limits the degradation process of these metallic materials.[6] The residual stress value in the oxide layers after cooling is often high (a few GPa in compression), and a relaxation process by delamination of the layer may occur, leading to an oxidation recovery due to spalling and causing damage to metal integrity. An accurate knowledge of the stress level in oxidized materials is thus required. Raman spectroscopy or X-ray diffraction (XRD) techniques are often used to determine residual stresses in the chromium oxide layer. In Table I, a non-exhaustive bibliographical synthesis of several works concerning stress measurements based on those two techniques is given.[7–23] It can be seen that even if the first works starting in 1986 are based on XRD, Raman spectroscopy has become the main technique to measure residual stresses today. However, to our knowledge, these two techniques have not been systematically used together to study residual stresses in the same thermal oxide/metal system. The underlying physical phenomena related to the measurements done with these two methods are totally different, and thus, the comparison of the results deduced from both techniques is essential for quantitative and accurate determination of stress levels. While Raman microspectroscopy using a confocal microscope can easily determine local stress at the micron scale, conventional X-Ray diffraction available in most laboratories probes the material with a beam size of about 1 mm in order to get a reasonable signal over noise ratio. At third generation synchrotron facilities, diffraction beamlines delivering intense submicrometer poly- and monochromatic X-ray beams have been developed for stress mapping over large areas of several tens of microns with high spatial resolution in complex materials containing several phases and a broad range of grain sizes.[24,25]

In this work, a multiscale approach has been adopted to accurately determine residual stresses in both adherent and damaged parts of the chromium oxide layer. To reach this goal, Raman spectroscopy and XRD techniques have been chosen and employed on the same specimens since these techniques are non-destructive. At the macroscopic scale, residual stress magnitudes in adherent parts of the scale are determined by conventional XRD and Raman spectroscopy. At the microscopic scale, residual stress maps over different types of delaminations are performed by Raman microspectroscopy and Synchrotron micro-diffraction. With the X-ray penetration depth being larger than the oxide layer thickness, the structural state of both the substrate, close to the interface, and the layer has also been studied in the Laue diffraction mode.

## II. EXPERIMENTAL

### A. Sample preparation

The detailed compositions of the Ni-30Cr and Fe-47Cr polycrystalline alloys used in the present study are given in Table II. With these compositions, oxide scales of the $\alpha$-$Cr_2O_3$ phase are formed at high temperature in open air. The samples were prepared keeping the same metallurgical conditions as used in Ref. 26]: for both alloys, we performed a thermal pre-treatment at 1000 °C during 1 h in open air to homogenize the metal. Then, plane disks with cylindrical geometries, 12 mm diameter and 1.5 mm thickness, were cut. All the sample surfaces were mechanically prepared with SiC paper and diamond paste to obtain a 3 $\mu$m metallic polishing finish which corresponds to an RMS roughness value of about 10 nm. Oxidations were done in a muffle furnace for temperatures ranging from 900 to 1000 °C and with an annealing time of 3 to 18 h. Cooling down to room temperature was performed in open air using different substrates for varying the cooling rate in the range of 80–500 °C/min. The oxide thickness obtained by thermo-gravimetric analysis increases with annealing temperature and time from 0.5 up to 3.7 $\mu$m for Ni-30Cr alloys and from 0.6 up to 8.6 $\mu$m for Fe-47Cr alloys.

### B. Sin$^2\psi$ method for residual stress determination by XRD

The well-known $\sin^2\psi$ method was applied for stress measurements in the texture-free polycrystalline oxide layers, $\psi$ being the angle between the sample surface normal and the (hkl) diffracting plane ones. Let us recall that in diffraction techniques, the interatomic distance d for a particular (hkl) plane is taken as a strain gauge; its $\psi$ angle dependence allows calculating the stress. Considering an equi-biaxial in-plane stress state in the oxide layer (stress-free surface, i.e., $\sigma_{33}=\sigma_{13}=\sigma_{23}=0$) and the rational definition of strains, the $\sin^2\psi$ relation becomes[27]

$$\ln\left(\frac{1}{\sin\theta}\right)=\left\{\frac{S_2(\mathrm{hkl})}{2}\sigma\right\}\sin^2\psi+2S_1(\mathrm{hkl})\sigma-\ln(\sin\theta_0), \quad (1)$$

where $\sigma$ is the in-plane residual stress, $\frac{1}{2}S_2(hkl)=\frac{1+\nu_{ox}}{E_{ox}}$ and $S_1(hkl)=-\frac{\nu_{ox}}{E_{ox}}$ are the X-ray elastic constants, $\theta$ is the strained diffraction angle, $\theta_0$ is the stress-free diffraction angle, $E_{ox}$ is the Young modulus of the oxide layer related to measured (hkl) planes, and $\nu_{ox}$ is the associated Poisson's ratio. XRD is thus sensitive to the elastic anisotropy of the material.

Taking into account Bragg's law

$$2\,d\,\sin\Theta=\lambda, \quad (2)$$

where $\lambda$ is the X-ray wavelength, $1/\sin\Theta$ and $1/\sin\Theta_0$ can be replaced in Eq. (1) by the strained interatomic distance d and the stress-free interatomic distance $d_0$, respectively.

XRD measurements have been done for the (116) diffracting planes of the oxide layer (Fig. 1) since the intensity and the angular position of the corresponding diffraction peak are high enough to be sensitive to the shift of the diffraction peak as a function of $\psi$ and thus to ensure accurate determination of related stresses. Let us note that the values of measurement parameters such as the angular step size (0.03°–0.04°) and recording time per step (20–35 s) depend on the oxide layer thickness and the geometrical

TABLE I. Residual stresses in chromium oxide as determined by different authors between 1986 and 2012 years using Raman spectroscopy or XRD.

| Authors | Year | Substrate | Temperature (°C) | $\sigma_r$ (GPa) | Method |
|---|---|---|---|---|---|
| Zhao[3,4] | 1986 | Ni-34Cr/Ni-34Cr-Y | 900 | −2 | XRD |
| Behnken[5] | 1988 | Inconel | 950 | −3.3 | XRD |
| Hou[6] | 1991 | Ni-25Cr | 1000 | −1.25 | XRD |
| Liu[7] | 1991 | Ni-Cr | 900 | −1.1 to −2.8 | XRD |
| Bennett[8] | 1992 | Cr | 875 | −0.2 | XRD |
| Birnie[9] | 1992 | 20-Cr-25Ni-Nb-steel | 800 | −0.98 | Raman |
| Goedjen[10] | 1994 | Cr | 940 | −1.234 | XRD |
| Daghigh[11] | 1996 | Ni-30Cr | 900 | −1.2 to −2.6 | XRD |
| Zhu[12] | 1997 | Ni-30Cr | 900 | −1.7 | XRD |
| Calvarin[13] | 1998 | Ni-30Cr | 900 | −2 to −3.5 | Raman |
| Mougin[14] | 2001 | Fe-18 Cr | 900 | −1.8 to −3 | Raman |
| Mougin[15] | 2001 | Fe-18Cr-TiNb | 900 | −1.6 to −2.9 | Raman |
| Mougin[16] | 2001 | Cr | 900 | −0.8 to −1.3 | Raman |
| Toscan[17] | 2004 | Fe-18Cr-X | 850 | −1.22 to −3.32 | Raman |
| Kemdehoundja[18] | 2006 | Ni-30Cr | 700–900 | −1 to −3 | Raman |
| Barnard[19] | 2010 | Ni-20Cr-4Fe | 800 | −1.4 to −1.8 | XRD |
| Barnard[19] | 2010 | Ni-23Cr-14W | 800 | −1.2 to −1.7 | XRD |

configuration of the measurement ($\psi$ value). Their values are chosen to optimize the signal to noise ratio. For stress determination, the following values for the corresponding X-ray elastic constants have been used: $\nu_{116} = 0.264$ and $E_{116} = 334.5$ GPa. They are obtained by averaging the Reuss and Voigt limits calculated by Panicaud *et al.*[28] from the single crystal elastic constants.[29] All the oxide layers investigated in the present work do not show any crystallographic fiber texture, the relative diffraction peak intensities being similar to the ones of the powder diffraction files given by the International Center for Diffraction Data (ICDD-PDF file No. 38–1479). Seven $\psi$ values (0°, 20.705°, 30°, 37.761°, 45°, 52.239°, and 60°) have been chosen to obtain equidistant points in the $\sin^2\psi$ range between 0 and 0.8. In order to take into account the instrumental errors, XRD patterns measured for a stress-free silicon powder sample from the National Institute of Standards and Technology (NIST) have been recorded for the same seven $\psi$ angles. An example of a $\sin^2\psi$ plot is given in Fig. 2 for two different annealing temperatures, i.e., two different residual stress states. The linearity predicted by Eq. (1) is experimentally confirmed and the slope which is related to the in-plane residual stress is negative (compression) and increases with temperature. Furthermore, the XRD measurements have been done for positive and negative $\psi$ values in order to check the presence or absence of in-plane shear stresses.[27] The two curves behave linearly and overlap at $\psi$=0, meaning that the assumption of in-plane isotropic residual stress state is verified. The uncertainty is estimated to be 0.15 GPa taking into account instrumental errors and the fitting procedure applied to the diffraction peak profile for extracting the peak position.

TABLE II. Chemical composition of NiCr-30 and FeCr-47 determined by electron probe micro-analysis.

| Elements | Ni | Cr | Si | Mn | C | P | S | Fe | N |
|---|---|---|---|---|---|---|---|---|---|
| NiCr-30 | 69,65 | 30,22 | <0,01 | <0,01 | 230 ppm | 30 ppm | 40 ppm | … | … |
| FeCr-47 | 0.25 | 47.35 | 0.1 | 0.02 | 200 ppm | … | 90 ppm | 52.35 | 0.01 |

### C. Micro-Raman spectroscopy

A high-resolution spectrometer - XY Dilor-Jobin Yvon (Horiba group) - has been used. The exciting source is a helium-neon laser working at a maximal power of 10 mW with a wavelength of $\lambda = 632.817$ nm. The Raman spectrum of the chromium oxide shows at room temperature four $E_g$ modes and one $A_{1g}$ mode. A typical spectrum for the oxide layer is shown in Fig. 3. The $A_{1g}$ vibration line which is the most intense corresponds to an isotropic optical mode and is then used for stress determination thanks to its sensitivity to the piezo-spectroscopic effect. The difference between the position $\nu$ of this line for an oxide layer under stresses $\sigma$ and its position $\nu_0$ for a stress-free material is linked to the stress $\sigma$ by the following equation:[30]

$$\sigma = 0.307 \pm 0.005 \times \Delta\nu. \quad (3)$$

Concerning the macroscopic stress evaluation, fifteen spectra measured in different areas where the oxide layer is adherent to the substrate have been treated. The mean value of $\Delta\nu$ then obtained gives the residual stress magnitude in the film. The $\nu_0$ value is evaluated using a powder made of a scrapped $\alpha$-$Cr_2O_3$ layer. Positions of A1g lines are extracted from Gauss/Lorentz fitting of the measured spectra vibration lines after background subtraction.

One major hypothesis of this method in thin films is related to the calibration procedure which allows determining the stress by measuring the shift of the Raman line. Indeed, the frequency shift calibration is obtained by applying three-dimensional hydrostatic pressure to a reference oxide powder, while the stress configuration for layers is two-dimensional with an out-of-plane zero stress-state at the free surface of the coating. A correction factor of 1.5 is then introduced in the equation giving the hydrostatic stress as a function of the Raman line shift in order to take into account

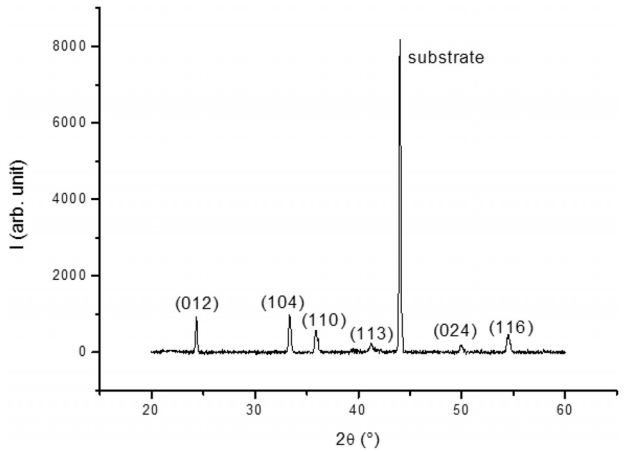


FIG. 1. Typical Θ–2Θ diffraction pattern of thermally grown chromium oxide layers measured at room temperature with a conventional laboratory diffractometer working with copper Kα radiation. A strong and flat background level principally due to chromium fluorescence (and also iron in the case of Fe-based alloys) when copper radiation is used has been subtracted. The substrate peak here corresponds to the (110) diffracting planes of the Fe-based body-centered cubic structure ($2\Theta = 44.674°$ for pure Fe: ICDD-PDF file No. 6-696).

this configuration change when measuring biaxial stresses in oxide layers [Eq. (3)]. Furthermore, this method does not allow to take into account the elastic anisotropy of the oxide phase contrary to XRD which seems then more precise but in turn more difficult to carry out.

## III. RESIDUAL STRESSES IN THE ADHERENT OXIDE LAYER

At the macroscopic scale, residual stress magnitudes are determined by conventional XRD using the $\sin^2\psi$ method and Raman spectroscopy. The influence of the oxidation conditions on residual stresses in the scale is investigated.

### A. Conventional X-ray diffraction

A 4-circle X-ray diffractometer from Seifert (GE) manufacturer - XRD 3000 - has been employed for XRD stress measurements. This setup is equipped with a copper Kα X-ray tube and a rear graphitic monochromator to eliminate iron fluorescence emanating from the sample. The size of the X-ray beam on the sample surface was about 2 $mm^2$, and its penetration depth at 8 keV was larger than the thickness of the oxide layers (between 0.5 and 8.6 μm) formed at the surface of the alloys.

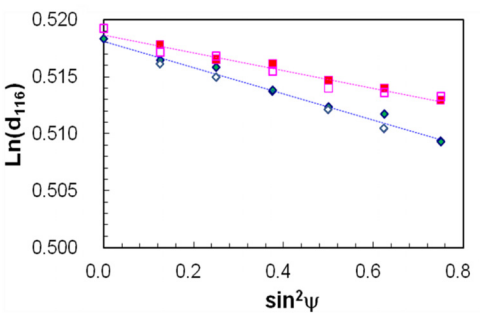


FIG. 2. $\mathrm{Sin}^2\psi$ plots for chromium oxide layers grown at 1000 (diamond-shaped) and 900 °C (square-shaped) on Ni-30Cr alloys. Full and empty symbols correspond to $\psi+$ and $\psi-$ angles, respectively.

### B. Comparison between Raman spectroscopy and X-ray diffraction

Residual stress investigations are carried out for both Ni-30Cr/$Cr_2O_3$ and Fe-47Cr/$Cr_2O_3$ systems using these two methods. The results are reported in Tables III and IV for all the studied samples. First, all the residual stresses are compressive with a magnitude ranging from 1.35 to 3 GPa depending on the oxidation conditions, the magnitude being larger at high temperature in agreement with the thermal stress contribution increase. Let us remark also that these stress amplitudes are comparable to the ones reported in Table I. Second, the correlation between values obtained with XRD and Raman spectroscopy (less than 100 MPa difference) is satisfying, which indicates that both techniques give good estimates of the residual stress magnitude in the chromium oxide films. It can be seen from both the NiCr and FeCr alloys that the stress (in absolute value) increases with the oxidation temperature and with the cooling rate up to 250 °C/min; then, it remains constant at higher cooling rates. This dependence has been analyzed in detail in Ref. 31. It has been shown that the maximum stress relaxation amplitude is obtained for the slower cooling rates, which is probably the consequence of the activation of non-destructive relaxation mechanisms occurring into the ceramic layer, such as viscoplastic-creep. Conversely, the delaminated surface fractions are maximum for the highest cooling rates.

The good agreement between these two techniques indicates the absence of the in-depth stress gradient in the oxide layer since the X-ray penetration depth is always larger than the oxide layer thickness in contrast to Raman spectroscopy where less than 1 μm in depth is probed. Furthermore, the different probe size used for macro stress determination, i.e., 1–2 μm for Raman and 1 mm for X-rays, indicates that the contribution to the total stress of delimitated areas is negligible. Let us recall that each Raman analysis for macro stress determination is repeated at least 12 times at different in-plane locations of the adherent oxide layer in order to obtain a representative macro stress value.

From Eq. (1), an interesting parameter can be derived using the $\sin^2\psi$ method: the stress-free inter planar distance $d_0$. It is equivalent to the distance in a free-standing (i.e.,

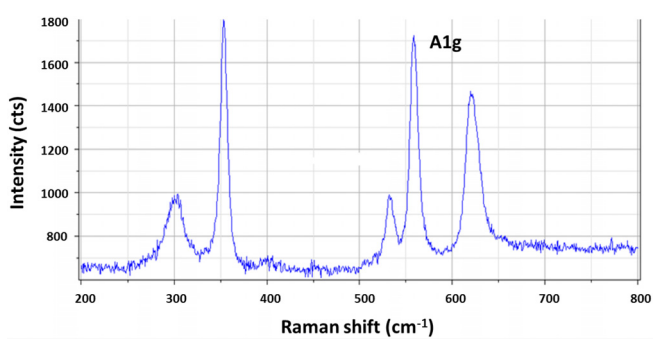


FIG. 3. As-measured typical Raman spectrum of the α-$Cr_2O_3$ phase under stress.

stress-free) oxide layer but without removing it from the substrate which is almost impossible. Table V summarizes the values obtained for all the samples studied in this work. The agreement between all values is remarkable within the uncertainties (standard deviation of 0.0001 nm) and clearly indicates that the oxide phase structure is similar whatever the oxide-forming alloys. It also demonstrates the rather good quality of XRD measurements and analysis done in this study.

## IV. RESIDUAL STRESSES ACROSS LOCAL DAMAGES

Raman micro-spectroscopy with its small probe size (2 $\mu m^2$) can also analyze stress at a local scale. It is thus possible to obtain stress maps related to delamination figures. For comparison, and in order to get reliable residual stress values, it is necessary to carry out synchrotron micro-diffraction experiments in identical oxide film regions.

Thus, residual stress mapping has been performed at the microscopic scale through different types of delaminations on the same specimens with both Raman micro-spectroscopy and synchrotron micro-diffraction. In the latter case, the ability to switch the X-ray beam from poly- to monochromatic radiation, while keeping the beam at the same place on the sample surface, allows studying both the substrate and the oxide scale.

### A. Synchrotron micro-diffraction

Synchrotron experiments have been performed on beamline 12.3.2 at the Advanced Light Source (ALS) Berkeley[24] and beamline BM32 at the European Synchrotron Radiation Facility (ESRF), Grenoble.[25] Both instruments achieve an X-ray spot size on the sample of 1 $\mu m^2$ through elliptically bent Kirkpatrick-Baez focusing mirrors. An MAR CCD detector was used at ESRF, and a DECTRIS Pilatus 1 M pixel array detector was used at ALS. The beam energy ranges from 6–14 keV at the ESRF and 6–22 keV at the ALS. The sample is placed on an XY stage and can therefore be raster scanned under the X-ray micro-beam. At each step, a diffraction pattern is collected via the 2D detector. The 2D diffraction patterns are analyzed using the XMAS software developed at the ALS. Feasibility tests with commercial chromium oxide powders have been first performed using micro-beam XRD (Fig. 4). The test indicates that Laue patterns would be in principle possible from the growing oxide. Indeed, for such powder and also for the oxide films, the grain size (deduced for the films from AFM topological surface measurements) is in a range [0.1;−1 $\mu$m], well adapted for white micro-beam.

TABLE III. Stress level in GPa measured by XRD. In all cases, stresses are compressive. The minimum absolute value corresponds to the stress level determined for the lower cooling rate of 80 °C per minute, while the maximum value corresponds to higher cooling rates of 500 °C per minute.

| | 3 h | 18 h. |
|---|---|---|
| Ni-30Cr/$Cr_2O_3$ | | |
| 900 °C | −1.90, −2.05, −2.20, −2.25 | −2.10, −2.50 |
| 1000 °C | −2.35, −3.05 | −2.65, −3.30 |
| Fe-47Cr/$Cr_2O_3$ | | |
| 900 °C | −1.40, −1.75 | −1.10, −1.40 |
| 1000 °C | −1.80, −2.00 | −1.15, −1.55 |

TABLE IV. Stress level in GPa measured by Raman spectroscopy. In all cases, stresses are compressive. The minimum absolute value corresponds to the stress level determined for the lower cooling rate of 80 °C per minute, while the maximum value corresponds to the higher cooling rates of 500 °C per minute.

| | 3 h | 18 h |
|---|---|---|
| Ni-30Cr/$Cr_2O_3$ | | |
| 900 °C | −1.85, −2.15, −2.25, −2.3 | −2.05, −2.40 |
| 1000 °C | −2.35, −3.00 | −2.85, −3.25 |
| Fe-47Cr/$Cr_2O_3$ | | |
| 900 °C | −1.35, −1.75 | −1.10, −1.40 |
| 1000 °C | −1.80, −1.95 | −1.35, −1.60 |

However, diffraction peak broadening analysis (not shown) has also been done for the oxide films to get the microstrains (lattice distortions) and the coherently diffracting domain (CDD) size and reveals that CDD is significantly smaller than the apparent grain sizes obtained with AFM (10 times smaller): from 0.07 to 0.12 $\mu$m when the oxidation temperature increases from 900 to 1000 °C, for both the Fe-47Cr and Ni-30Cr substrates.[32] The XRD experiments have been done in the Θ–2Θ mode, which means that the direction of the measurements is perpendicular to the sample surface. However, the $\sin^2\psi$ analysis done with a four circle X-ray diffractometer does not reveal a strong variation of the diffraction peak profile with respect to the $\psi$ angles except at large $\psi$ values due to geometrical consideration (enlargement of the X-ray illuminated area). This indicates that the CDD sizes are almost equivalent in all space directions. To conclude, two approaches have been used to estimate the size of the crystallites/grains by applying XRD and AFM measurements on the same samples. The AFM observations [see, for instance, Fig. 1(c) in Ref. 5 and Fig. 2(a) in Ref. 33] allow estimating the in-plane grain size from the morphology at the free sample surface which is a rough estimate of the grain size and cannot be compared directly to CDD sizes since the latter is related to crystals with zero defects.

This explains why no meaningful Laue patterns could be obtained from the oxide films using white beam measurements (too low number of Laue spots and too high number of grains). On the other hand, the signal originating from the underlying substrate was exploitable and allows us to map the substrate grain orientation as shown in Figs. 5 and 6, both above adherent regions and delaminated areas. The phi Euler angle distribution obtained from analysis with the XMAS software permits us to calculate the grain disorientation distribution with respect to the sample axis. Such an Euler angle map is equivalent to the substrate grain orientation under the oxide film and can be compared to the one obtained from an Electron Backscatter Diffraction (EBSD) analysis. However, the latter technique is not applicable to the present case because of the too strong electron absorption through the oxide layer. Laue X-ray microdiffraction can therefore probe the substrate in-plane grain size distribution under delaminated areas, and the results indicate that buckles may form and reach dimensions spanning over several

TABLE V. Summary of the stress-free inter planar distances $d_0$ for (116) diffracting planes determined par XRD for all chromia layers. The reference value is 0.16724 nm (ICDD-PDF file N° 38-1479).

| Metallurgical parameters: Annealing temperature (°C) and time (h), cooling rate (°C/min) | $d_0$ (nm) | |
|---|---|---|
| | Ni-30Cr/$Cr_2O_3$ | Fe-47Cr/$Cr_2O_3$ |
| 900, 3, 80 | 0.16743 | 0.16726 |
| 900, 3, 500 | 0.16705 | 0.16732 |
| 900, 18, 80 | 0.16729 | 0.16724 |
| 900, 18, 500 | 0.16727 | 0.16719 |
| 1000, 3, 80 | 0.16733 | 0.16718 |
| 1000, 3, 500 | 0.16718 | 0.16709 |
| 1000, 18, 80 | 0.16740 | 0.16727 |
| 1000, 18, 500 | 0.16722 | 0.16709 |
| Average | 0.16727 | 0.16720 |

substrate grains. This is the case, for example, in Fig. 5 for NiCr-30 after 3 h upon oxidation at 900 °C (the red boxed area corresponds to the mapped zone). Delaminations can also be localized above a single substrate grain. This is the case in Fig. 6 for the system $Cr_2O_3$/Fe-47Cr after 18 h upon oxidation at 1000 °C (the mapped zone was larger than the dimensions of the micrograph). It should be mentioned that the substrate grain size in Fe-47Cr is about 100 to 200 $\mu$m, while it is only 20–50 $\mu$m in Ni-30Cr. The main result here is that a delamination situation may occur either above several substrate grains or above one unique grain. Thus, the presence or absence of grain boundaries has no significant influence on the delamination initiation and localization processes. On the contrary, buckle propagation is certainly very sensitive to the substrate grain size and more precisely to thermomechanical property anisotropy of the metallic alloy. Indeed, an elongated spall shape has been previously observed for Fe-47Cr alloys.[32–34] As shown in Fig. 6, delamination may propagate on a single grain giving rise to a circular buckle. In that case, the residual-stress state is equi-biaxial which means that the in-plane thermomechanical properties of the single crystal are isotropic. This is not always the case since thermomechanical properties are grain orientation dependent and thus non equi-biaxial in-plane stress state in the oxide scale may develop on cooling for a particular single grain orientation leading then to the asymmetric shape of the buckle. However, confirmation of this hypothesis needs further bi-axial stress measurements on a large number of buckles for both alloys including asymmetric ones.

In order to get a reliable diffraction signal from the oxide scale, monochromatic X-ray beams with a larger probe size compared to the polychromatic mode have been used: the beam was about 4 $\mu m^2$ at ESRF Grenoble and $7\times2$ $\mu m^2$ at ALS Berkeley. The monochromatic beam is obtained by inserting a monochromator in the path of the white beam. Typical Debye-Scherrer diffraction rings are shown in Fig. 7 for a commercial chromium oxide powder. In the case of chromium oxide layers, only the diffraction signal given by the Fe-47Cr alloys oxidized 18 h oxidation at 1000 °C was detectable. Bucklings have been mapped in XY using the monochromatic beam, and Debye-Scherrer ring patterns were obtained at each scan step. Because of the poor quality of the Debye-Scherrer diffraction diagrams, due to the low coating thickness, an integration of the diffraction pattern has been done for each horizontal line of the XY map. The resulting X-ray patterns are then analyzed applying the $\sin^2\psi$ method.[30] Consequently, an average residual stress profile through the buckle is obtained along a vertical line in Fig. 8. In that case, the in-plane residual stress magnitude just around the buckling is about −1.5 GPa. These values decrease to about −0.6 to −0.2 GPa at the top of the buckle. The stress released region is about 70 $\mu$m diameter. Let us note that the stress magnitude measured in the adherent part around the buckle is close to the one obtained with macroscopic measurements (see paragraphs 3.1 and 3.2).

### B. Stress distribution from Raman micro-spectroscopy maps

The Raman spectrometer coupled with an autofocus device leads to a high spatial resolution. This equipment gives access to three sets of information from the same part of the oxide film: an optical image giving, e.g., the size of the debonded zone, the local stress distribution, and the height profile above the oxide/substrate interface. It has been observed that buckles have often a quasi-circular shape and that the mean diameter increases from 10 to 15 $\mu$m to about 100 $\mu$m, during buckle propagation. The experimental conditions leading to the formation of buckles and spalls can be characterized by the oxidation parameters: oxidation time and temperature and cooling rate.[5] Raman spectra obtained from chromium oxide films (Fig. 3) are of sufficient good

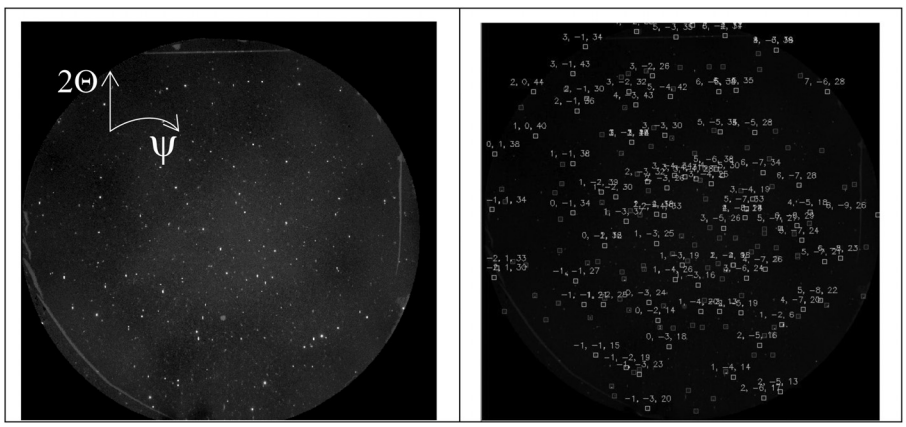


FIG. 4. Laue patterns of commercial chromium oxide powder after background subtraction (left) and 90 peaks indexation (right).

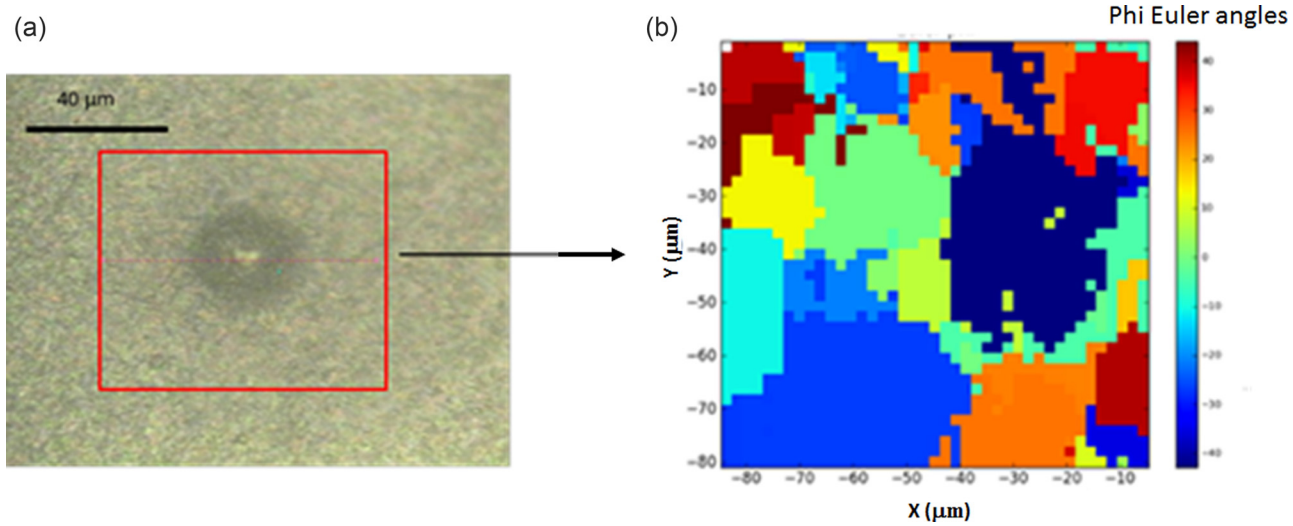


FIG. 5. Ni-30Cr/$Cr_2O_3$ system after 18 h oxidation at 1000 °C: (a) optical image of a buckle and (b) corresponding crystallographic grain orientation map (phi Euler angle) of the substrate under the delaminated film area.

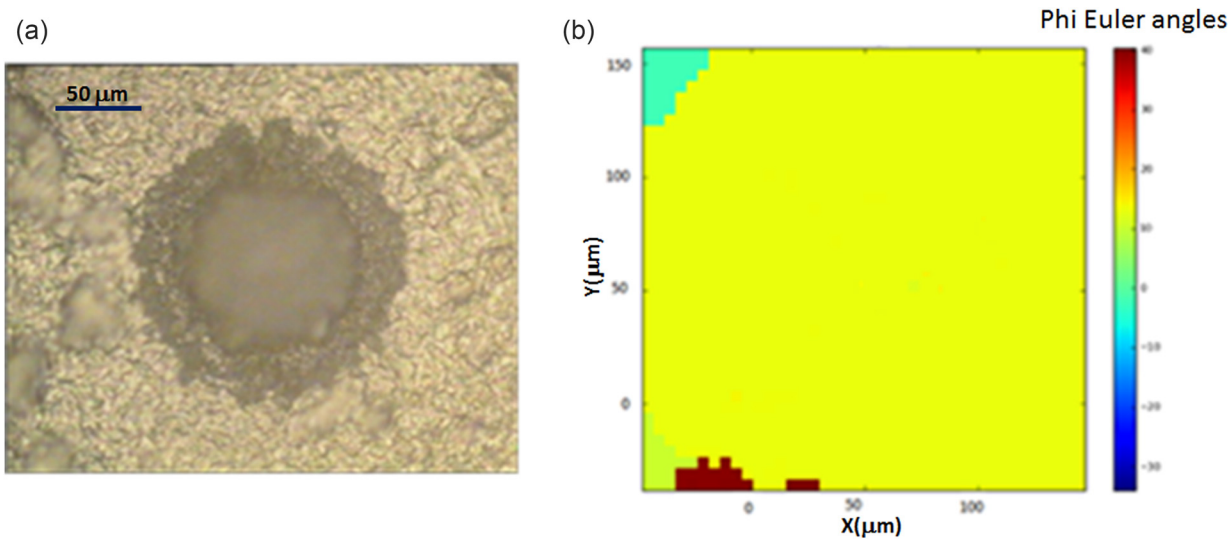


FIG. 6. Fe-47Cr/$Cr_2O_3$ system after 18 h oxidation at 1000 °C: (a) Optical image of a buckle and (b) corresponding crystallographic grain orientation map (phi Euler angle) of the substrate under the delaminated film area.

quality for an acquisition time of 15 s. Such low acquisition time permits obtaining two-dimensional maps through damaged zones of the oxide films in less than a few hours. The horizontal measurement increment can be reduced to 2 $\mu$m, with a lateral probed zone of 2 $\mu m^2$. In order to map with a good accuracy the same delaminated object by using either micro-Raman or micro-XRD, it has been necessary to mark some buckles for easy localization. It has been done by doing indentation mark far away from the buckles to make sure that such an indentation procedure will not perturb the strain/stress distribution around the buckles. For the system Fe-47Cr/$Cr_2O_3$ after 18 h at 1000 °C, the corresponding buckles (Fig. 9) give rise to in-plane stress magnitudes between −1.5 and −2 GPa close to the buckle. At the top, it is between −0.5 and 0 GPa. The stress released areas are comparable to the one obtained from micro-diffraction measurements (Fig. 8). Overall, the two techniques give similar results.

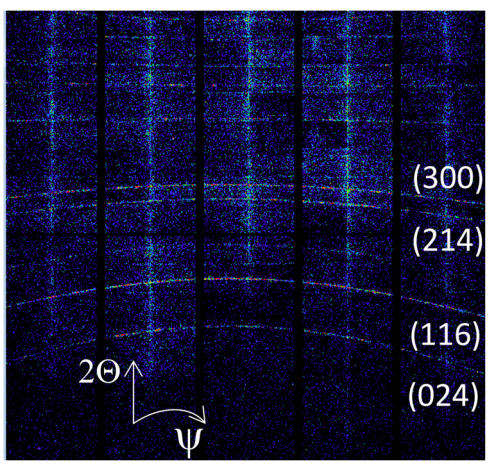


FIG. 7. Monochromatic 2D XRD diagram of a commercial α-$Cr_2O_3$ chromium oxide powder.

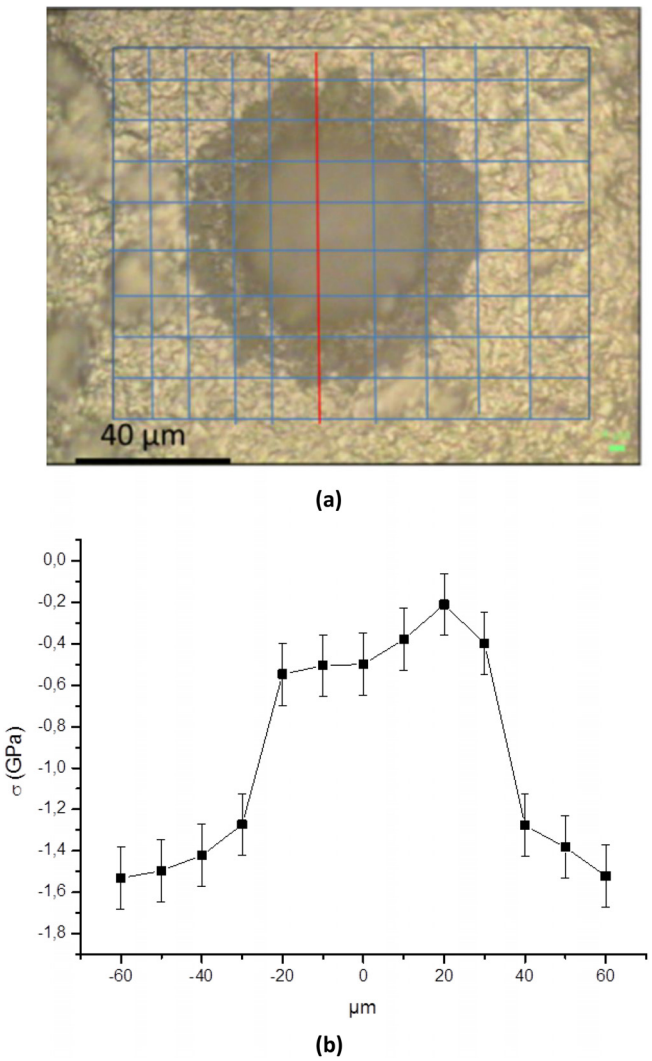


FIG. 8. Fe-47Cr/$Cr_2O_3$ system after 18 h at 1000 °C: (a) Optical micrograph of a buckling observed on the chromia layer and (b) corresponding micro-XRD stress profile (along a vertical red line).

However, Raman micro-spectroscopy presents some advantages: maps are obtained from a larger number of measurement points and offer better a spatial resolution and a better signal-to-noise ratio than monochromatic X-ray microdiffraction. The data analysis is also more straightforward.

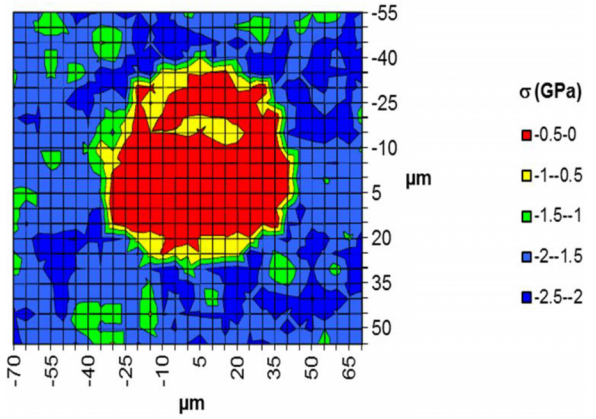


FIG. 9. Stress map obtain by Raman micro-spectroscopy over a buckle observed for a chromia layer in the Fe-47Cr/$Cr_2O_3$ system after 18 h oxidation at 1000 °C.

## V. CONCLUSION

Residual stress distribution in chromium oxide films grown on both Fe-Cr and Ni-Cr substrates has been studied as a function of oxidation temperature, oxidation duration, and cooling rate. For the first time, both X-ray diffraction and Raman spectroscopy have been used on the same samples at micro and macro length scales. The results obtained with both techniques at a macroscopic scale in the adherent parts of the films are in agreement. At the local scale, white beam micro-diffraction experiments show that buckles are located either over several substrate grains or on a single grain, indicating that the crystalline orientation and size of the substrate grains do not influence buckle nucleation and growth. Residual stresses have been determined locally through delaminated areas in oxide films using X-Ray monochromatic micro-beam and Raman micro-spectroscopy. The stress magnitudes and distribution obtained by both techniques are also in good agreement at this scale and show a high stress release between the top of a buckle and the adherent part. Because of its simplicity of use, Raman micro-spectroscopy will be favored in further studies for a detailed analysis of damaging by delamination in chromium oxide films, in the framework of thin plate theory used for buckling mechanic analysis. Finally, Laue micro-diffraction experiments reveal the polycrystalline structure of the substrate under damages occurring in the oxide scale and thus bring new insight into the asymmetric morphology (elongation) of some buckling, which may be attributed to elastic anisotropy of large single crystals in polycrystalline Fe-47Cr alloys.

## ACKNOWLEDGMENTS

We wish to thank the ESRF for providing the X-ray source. Beamline 12.3.2 and the Advanced Light Source were supported by the Director, Office of Science, Office of Basic Energy Sciences, of the U.S. Department of Energy under Contract No. DE-AC02–05CH11231.

[1]N. Birks and H. Rickert, J. Inst. Met. **91**, 308 (1962/63).
[2]K. Hauffe, *Oxidation of Metals (Translation from German)* (Plenum Press, New York, 1965).
[3]P. Kofstad, *High-Temperature Oxidation of Metals* (Wiley, New York, 1966).
[4]O. Kubaschewski and B. E. Hopkins, *Oxidation of Metals and Alloys*, 2nd ed. (Butterworth, London, 1967).
[5]M. Guerain, J.-L. Grosseau-Poussard, and P. Goudeau, J. Appl. Phys. **113**, 063502 (2013).
[6]A. M. Huntz and B. Pieraggi, *Oxydation Des Matériaux Métalliques* (Hermes-Lavoisier, 2003).
[7]J.-G. Zhao, A.-M. Huntz, P. Couffin, and J.-L. Baron, Acta Metall. **34**, 1351 (1986).
[8]J.-G. Zhao, Ph.D. thesis, Université Paris XI, Orsay, France, 1986.
[9]H. Behnken and V. Hauk, *International Conference on Residual Stresses (ICRS 2)*, edited by G. Beck, S. Denie, and A. Simon (Elsevier Applied Science, London, 1988), p. 341.
[10]P. Y. Hou and J. Stringer, Acta Metall. **39**, 841 (1991).
[11]C. Liu, Ph.D. thesis, ENSAM Paris, France, 1991.
[12]M. J. Bennett, in *Proceedings of the International Symposium on Solid State Chemistry of Advanced Materials and Protective Coatings*, Tokyo, Japan, edited by Y. Saito, B. Onay, and T. Maruyama (Elsevier Amsterdam, 1992), p. 51.
[13]J. Birnie, C. Craggs, D. J. Gardiner, and P. R. Graves, Corros. Sci. **33**, 1 (1992).

[14]J. G. Goedjen, J. H. Stout, G. Qiti, and D. A. Shores, Mat. Sci. Eng., A **177**, 115 (1994).
[15]S. Daghigh, Ph.D. thesis, Université Paris XI, Orsay, 1996.
[16]D. Zhu, J. H. Stout, and D. A. Shores, Mater. Sci. Forum **254**, 333 (1997).
[17]G. Calvarin, A. M. Huntz, A. Hugot Le Goff, S. Joiret, and M. C. Bernard, Scr. Mater. **38**, 1649 (1998).
[18]J. Mougin, PhD thesis, INP Grenoble (2001)
[19]P. Y. Hou, J. Ager, J. Moulin, and A. Galerie, Oxid. Met. **75**, 229–245 (2011).
[20]J. Mougin, A. Galerie, G. Lucazeau, and L. Abello, Mater. Sci. Forum **369–372**, 841 (2001).
[21]F. Toscan, Ph.D. thesis, INP Grenoble, 2004.
[22]M. Kemdehoundja, J. F. Dinhut, J. L. Grosseau-Poussard, and M. Jeannin, Mater. Sci. Eng., A **435-436**, 666 (2006).
[23]B. R. Barnard, T. R. Watkins, and P. K. Liaw, Oxid. Met. **74**, 305 (2010).
[24]N. Tamura, M. Kunz, K. Chen, R. S. Celestre, A. A. MacDowell, and T. Warwick, Mater. Sci. Eng. A **524**, 28 (2009).
[25]O. Ulrich, X. Biquard, P. Bleuet, O. Geaymond, P. Gergaud, J. S. Micha, O. Robach, and F. Rieutord, Rev. Sci. Instrum. **82**, 033908 (2011).
[26]M. Kemdehoundja, J. L. Grosseau-Poussard, and J. F. Dinhut, Appl. Surf. Sci. **256**, 2719 (2010).
[27]V. Hauk, *Structural and Residual Stress Analysis by Non Destructive Methods: Evaluation, Application, Assessment* (Elsevier, Amsterdam, 1997).
[28]B. Panicaud, Ph.D. thesis, La Rochelle University, France, 2004.
[29]H. L. Alberts and J. C. A. Boyens, "The elastic constants and distance dependence of the magnetic interactions of $Cr_2O_3$," J. Magn. Magn. Mater. **2**, 327–333 (1976).
[30]J. Mougin, T. Le Bihan, and G. Lucazeau, J. Phys. Chem. Solids **62**, 553 (2001).
[31]M. Guerain, P. Goudeau, and J. L. Grosseau-Poussard, J. Appl. Phys. **110**, 093516 (2011).
[32]M. Guerain, Ph.D. thesis, La Rochelle University, France, 2012.
[33]M. Guerain, F. Rakotovao, S. Y. Brou, G. Bonnet, B. Panicaud, J. L. Grosseau-Poussard, and P. Goudeau, J. Alloys Compd. **718**, 223 (2017).
[34]P. Goudeau, P. Villain, N. Tamura, and H. A. Padmore, Appl. Phys. Lett. **83**, 51–53 (2003).